# Critical Determinants of $Ca^{2+}$-Dependent Inactivation within an EF-Hand Motif of L-Type $Ca^{2+}$ Channels

Blaise Z. Peterson, Joanna S. Lee, Jennifer G. Mulle, Yan Wang, Marita de Leon, and David T. Yue
Program in Molecular and Cellular Systems Physiology, Departments of Biomedical Engineering and Neuroscience, Johns Hopkins University School of Medicine, Baltimore, Maryland 21205 USA

ABSTRACT L-type ($\alpha_{1C}$) calcium channels inactivate rapidly in response to localized elevation of intracellular $Ca^{2+}$, providing negative $Ca^{2+}$ feedback in a diverse array of biological contexts. The dominant $Ca^{2+}$ sensor for such $Ca^{2+}$-dependent inactivation has recently been identified as calmodulin, which appears to be constitutively tethered to the channel complex. This $Ca^{2+}$ sensor induces channel inactivation by $Ca^{2+}$-dependent CaM binding to an IQ-like motif situated on the carboxyl tail of $\alpha_{1C}$. Apart from the IQ region, another crucial site for $Ca^{2+}$ inactivation appears to be a consensus $Ca^{2+}$-binding, EF-hand motif, located ~100 amino acids upstream on the carboxyl terminus. However, the importance of this EF-hand motif for channel inactivation has become controversial since the original report from our lab implicating a critical role for this domain. Here, we demonstrate not only that the consensus EF hand is essential for $Ca^{2+}$ inactivation, but that a four-amino acid cluster (VVTL) within the *F* helix of the EF-hand motif is itself essential for $Ca^{2+}$ inactivation. Mutating these amino acids to their counterparts in non-inactivating $\alpha_{1E}$ calcium channels (MYEM) almost completely ablates $Ca^{2+}$ inactivation. In fact, only a single amino acid change of the second valine within this cluster to tyrosine (V1548Y) supports much of the functional knockout. However, mutations of presumed $Ca^{2+}$-coordinating residues in the consensus EF hand reduce $Ca^{2+}$ inactivation by only ~2-fold, fitting poorly with the EF hand serving as a contributory inactivation $Ca^{2+}$ sensor, in which $Ca^{2+}$ binds according to a classic mechanism. We therefore suggest that while CaM serves as $Ca^{2+}$ sensor for inactivation, the EF-hand motif of $\alpha_{1C}$ may support the transduction of $Ca^{2+}$-CaM binding into channel inactivation. The proposed transduction role for the consensus EF hand is compatible with the detailed $Ca^{2+}$-inactivation properties of wild-type and mutant V1548Y channels, as gauged by a novel inactivation model incorporating multivalent $Ca^{2+}$ binding of CaM.

## INTRODUCTION

L-type calcium channels inactivate most rapidly through a mechanism driven by an elevation of intracellular $Ca^{2+}$ within a few hundred angstroms of the channel pore. Such "$Ca^{2+}$-dependent inactivation" (Brehm and Eckert, 1978) provides vital $Ca^{2+}$ negative feedback in numerous settings, including the normal regulation of the cardiac action potential (Linz and Meyer, 1998), along with its abnormal prolongation in heart disease (O'Rourke et al., 1999; Winslow et al., 1999). As such, $Ca^{2+}$ inactivation of these channels has been an intense focus of research spanning more than two decades.

Over the past four years there has been rapid progress toward understanding the molecular basis for such inactivation. We showed that critical determinants of $Ca^{2+}$ inactivation were localized to the proximal third of the carboxyl terminus of the main $\alpha_{1C}$ subunit of L-type channels (de Leon et al., 1995), referred to as the *C*$a^{2+}$ *i*nactivation, or "CI" region (Peterson et al., 1999). The main supporting evidence was that deletion of the distal two-thirds of the $\alpha_{1C}$ carboxyl tail spared $Ca^{2+}$ inactivation; replacement of the $\alpha_{1C}$ CI region by the homologous region of a non-inactivating $\alpha_{1E}$ calcium channel (Soong et al., 1993) abolished $Ca^{2+}$ inactivation; and donation of the $\alpha_{1C}$ CI region to the $\alpha_{1E}$ backbone conferred $Ca^{2+}$ inactivation to the non-inactivating background (de Leon et al., 1995). In addition, substituting just 53 amino acids near the beginning of the $\alpha_{1C}$ CI region with the homologous sequence from $\alpha_{1E}$ eliminated $Ca^{2+}$ inactivation. This short stretch of $\alpha_{1C}$ contained a consensus $Ca^{2+}$-binding motif (EF hand) (Babitch, 1990), leading us to suggest that this domain contained a $Ca^{2+}$ sensor for $Ca^{2+}$ inactivation.

Subsequent work has confirmed and extended the evidence that the $\alpha_{1C}$ CI region figures critically in L-type channel inactivation by $Ca^{2+}$. By using similar chimeric channel analysis between $\alpha_{1C}$ and $\alpha_{1E}$, Zhou et al. (1997) confirmed the importance of the $\alpha_{1C}$ CI region, as substitution of the entire $\alpha_{1C}$ CI region into $\alpha_{1E}$ conferred $Ca^{2+}$ inactivation, while replacing proximal portions from the $\alpha_{1C}$ CI region failed to confer the inactivating phenotype. More recently, Soldatov et al. (1998) found that $Ca^{2+}$ inactivation was eliminated by simultaneous mutation of two stretches within the $\alpha_{1C}$ CI region (IKTEG and LLDQV), residing just downstream of the consensus EF hand by 51 and 79 residues. Finally, Zuhlke and Reuter (1998) used systematic deletions within the $\alpha_{1C}$ carboxyl tail to identify two additional sites within the CI region that are essential for $Ca^{2+}$ inactivation. Of these two groups of amino acids, NE and IQEYFRKF (61 and 103 residues downstream of the con-

*Received for publication 7 September 1999 and in final form 3 January 2000.*

Address reprint requests to Dr. David T. Yue, Program in Molecular and Cellular Systems Physiology, Depts. of Biomedical Engineering and Neuroscience, Johns Hopkins University School of Medicine, Ross Building, Rm. 713, 720 Rutland Ave., Baltimore, MD 21205. Tel.: 410-955-0078; Fax: 410-955-0549; E-mail: dyue@bme.jhu.edu.



0006-3495/00/04/1906/15 $2.00

sensus EF hand, respectively), the latter was notable, because it approximates the consensus pattern for an IQ calmodulin-binding motif (IQxxxRG) (Rhoads and Friedberg, 1997). This finding raised the possibility that calmodulin might play a role in $Ca^{2+}$ inactivation.

In the past year, we (Peterson et al., 1999) and others (Qin et al., 1999; Zuhlke et al., 1999) have demonstrated that calmodulin (CaM) is indeed the dominant $Ca^{2+}$ sensor for $Ca^{2+}$ inactivation of L-type channels. CaM appears to be constitutively tethered to the channel like an integral subunit, and further $Ca^{2+}$-dependent binding of tethered CaM to the IQ-like motif is an essential step for channel inactivation (Peterson et al., 1999; Zuhlke et al., 1999; Qin et al., 1999). Given the primacy of CaM as $Ca^{2+}$ sensor, and of the IQ-like domain as CaM binding site, what role do the other critical sites on $\alpha_{1C}$ play in the inactivation process?

This question is particularly relevant to the consensus EF hand, because the importance of this motif for $Ca^{2+}$ inactivation has become controversial. Although we and others found that either exchanging the EF-hand segment from $\alpha_{1C}$ with a homologous sequence from $\alpha_{1E}$ (de Leon et al., 1995), or deleting the EF-hand segment from $\alpha_{1C}$ altogether (Zuhlke et al., 1999) abolished $Ca^{2+}$ inactivation, Zhou et al. (1997) could not confirm these findings. The latter group also found that substitution of only the distal two-thirds of the $\alpha_{1C}$ CI region (not including the EF-hand motif) into $\alpha_{1E}$ was sufficient to impart $Ca^{2+}$ inactivation. Furthermore, mutation of residues presumed to coordinate $Ca^{2+}$ within an EF hand failed to reduce (Zhou et al., 1997), or only partially blunted, $Ca^{2+}$ inactivation (Bernatchez et al., 1998). These results call into question the importance of the consensus EF hand.

In this study we have therefore undertaken systematic mutagenesis of $\alpha_{1C}$ channels, where small segments of the $\alpha_{1C}$ EF-hand motif have been changed to their $\alpha_{1E}$ correlates in two to four residue clusters. Not only do we confirm that the consensus EF-hand motif is essential for $Ca^{2+}$ inactivation, we also identify a four-amino acid cluster (VVTL) within the *F* helix of the consensus EF hand that is itself essential for inactivation. Changing these residues to their $\alpha_{1E}$ analogs (MYEM) almost completely eliminates $Ca^{2+}$ inactivation, and point mutation of only the second residue in the cluster (V1548Y) mimics much of this effect. However, mutations of presumed $Ca^{2+}$-coordinating residues in the EF-hand motif reduce $Ca^{2+}$ inactivation by only ~2 fold, fitting poorly with the EF hand serving as a contributory inactivation $Ca^{2+}$ sensor, in which $Ca^{2+}$ binds according to a classic mechanism. We therefore suggest that, rather than serve as $Ca^{2+}$ sensor for inactivation, the consensus EF hand may be essential to the transduction of CaM binding into inactivation. A novel inactivation model, incorporating multivalent $Ca^{2+}$ binding of CaM, is used to evaluate the feasibility of the proposed transduction role for the EF-hand domain.

## METHODS

### Site-directed mutagenesis

The segment of $\alpha_{1C}$ cDNA (Wei et al., 1991) encoding the consensus EF-hand motif is flanked by recognition sequences for the restriction enzymes *Eco*RV at position 4566 and *Sfu*I at position 5191. The *Sfu*I recognition sequence was engineered by silent mutagenesis; 626-basepair DNA fragments containing mutations within the consensus EF-hand motif were generated by polymerase chain reaction (PCR) using mutagenic primers and the overlap extension strategy (Ho et al., 1989), and were subcloned into the shuttle vector, PCRSCRIPT (Strategene, La Jolla, CA). *Pfu* polymerase was used throughout. These plasmids were digested and the resulting *Eco*RV-*Sfu*I fragments were gel-purified (GeneClean, Bio 101, Vista, CA) and subcloned into *Eco*RV-*Sfu*I-digested $\alpha_{1C}$/pcDNA3. The integrity of all of the wild-type and mutant constructs used in this study was confirmed by qualitative restriction digests and sequence analysis. In particular, the $\alpha_{1CE\text{-}3}$ channel constructed previously (de Leon et al., 1995) was re-sequenced across the entire C-tail region subject to PCR.

### Rationale for point mutations in the consensus EF-hand

In EF hands, $Ca^{2+}$ is typically coordinated by six amino acids in the binding loop, with stereotypic coordinates as diagrammed at the top of Fig. 1 ($x$, $y$, $z$, $-y$, $-x$, and $-z$). To test whether the consensus EF hand in $\alpha_{1C}$ binds $Ca^{2+}$ according to a mechanism demonstrated by classic EF hands, we made individual point mutations at amino acids at the presumably crucial coordinating locations ($x$, $y$, $z$, and $-z$), as such point mutations reduce the $Ca^{2+}$ affinity of classic EF hands by 10–1000-fold (Linse and Forsen, 1995). Hence, our expectation was that, if $Ca^{2+}$ binding to the consensus EF hand triggers channel inactivation, then point mutations at these coordinates should severely attenuate $Ca^{2+}$ inactivation. The rationale for the choice of mutations was as follows. In the mutant channel D1535A, we substituted an alanine for the aspartate residue at position 1535 ($x$), which is conserved in all EF-hand proteins and high-threshold calcium channels. In the mutants E1537A and K1539C, we altered residues that correspond to coordinates $y$ and $z$ of the consensus EF hand from their identities in $\alpha_{1C}$ to those in $\alpha_{1E}$. The most impressive effects were expected of mutant D1546A, in which alanine was substituted for aspartate 1546, corresponding to the $-z$ coordinate, which contributes two $Ca^{2+}$-interaction ligands in classic EF hands. The alanine substitutions in mutants D1535A and D1546A would be most likely to attenuate $Ca^{2+}$ binding without disrupting the overall secondary structure of this segment. The residues corresponding to $-y$ and $-x$ coordinates were not altered, because carbonyl oxygen on the peptide backbone interacts with $Ca^{2+}$ at the $-y$ coordinate, and the side chain corresponding to $-x$ coordinate complexes with $Ca^{2+}$ indirectly via a water molecule (Falke et al., 1994). Consequently, the amino acid residues at these positions are highly variable in EF-hand proteins. Furthermore, arginine 1541 ($-y$) is conserved between $\alpha_{1C}$ and $\alpha_{1E}$, and could not have contributed to the reduction of $Ca^{2+}$ inactivation seen with the chimera $\alpha_{1CE\text{-}3}$. The results of the mutations described above are summarized in Fig. 2. The effect of lysine 1543 ($-x$) was assessed within the context of the cluster mutation KHL → HYT in Fig. 3.

### Electrophysiology

Whole-cell patch clamp recordings were acquired as described previously (Peterson et al., 1999). Briefly, complementary DNAs encoding wild-type or mutant $\alpha_{1C}$ calcium channel subunits were cotransfected with $\beta_{2a}$ (Perez-Reyes et al., 1992) and $\alpha_2\delta$ (Tomlinson et al., 1993) in HEK 293 cells by calcium phosphate precipitation, and whole-cell currents were recorded at room temperature 2–3 days after transfection. Bath solution

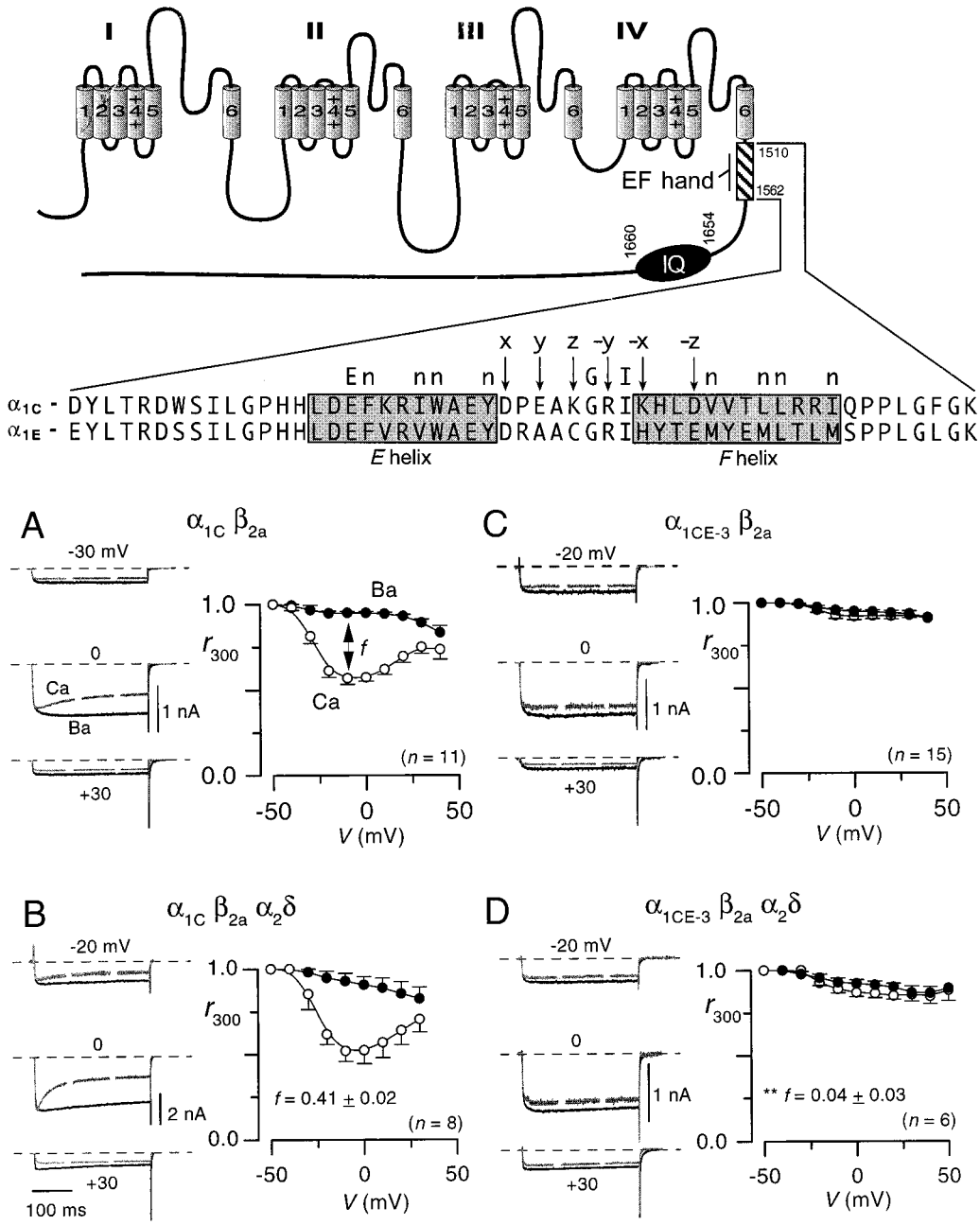


FIGURE 1 An EF-hand-containing segment in the carboxyl terminus of $\alpha_{1C}$ contains determinants that are critical for $Ca^{2+}$-dependent inactivation. *Top:* putative transmembrane folding model for the main subunit ($\alpha_{1C}$) of the L-type calcium channel. When a 53-amino acid segment in the carboxyl terminus (*hatched box*, amino acids 1510–1562 in $\alpha_{1C}$) is replaced by the analogous segment from $\alpha_{1E}$, the resulting chimera ($\alpha_{1CE-3}$) lacks $Ca^{2+}$-dependent inactivation. The primary sequences of $\alpha_{1C}$ and $\alpha_{1E}$ that correspond to this segment are aligned in the expanded view, below. A consensus EF-hand is identified using the Tufty-Kretsinger scoring method as indicated above the alignment where "n" denotes a hydrophobic amino acid, and amino acids that coordinate the $Ca^{2+}$ ion are designated *x*, *y*, *z*, $-y$, $-x$, and $-$z. The *E* and *F* helices of the EF-hand are identified using shaded boxes. An IQ-like domain (IQ), situated downstream of the consensus EF hand is also a crucial element in $Ca^{2+}$ inactivation. $Ca^{2+}$-dependent calmodulin binding to this element is an essential step in channel inactivation. (*A–D*) Inactivation properties of whole-cell current from cells overexpressing wild-type $\alpha_{1C}$ (*A, B*) or chimeric $\alpha_{1CE-3}$ (*C, D*) subunits, which illustrate the robustness of $Ca^{2+}$-dependent inactivation in wild-type channels and the loss of such inactivation in the chimeric channels. Only the $\beta_{2a}$ subunit was coexpressed with $\alpha_1$ in panels *A* and *C*. Both $\beta_{2a}$ and $\alpha_2\delta$ were coexpressed in panels *B* and *D*. The format of all panels is as follows. *Left:* exemplar $Ba^{2+}$ (*black*) and $Ca^{2+}$ (*gray*, *dashed*) currents elicited by depolarizing steps to the indicated potentials. Here and throughout the figures, $Ca^{2+}$ has been scaled upward ~3× to facilitate comparison of kinetics, and tail currents have been clipped for display clarity. *Right:* fraction of current remaining at the end of 300-ms depolarizations ($r_{300}$) is plotted as a function of depolarizing potentials, with $Ba^{2+}$ (*closed circles*) or $Ca^{2+}$ (*open circles*) as the charge carrier. *f* is the difference between $Ba^{2+}$ and $Ca^{2+}$ $r_{300}$ values at $-10$ mV, diagrammed in *A*. This parameter, which functions as a concise measure of the strength of $Ca^{2+}$-dependent inactivation, is reported at the bottom of $r_{300}$ graphs in *B* and *D*. Here, and in all the figures, $r_{300}$ and *f* data are displayed as mean ± SEM and averaged from the number of cells indicated in parentheses. Statistically significant reductions in $Ca^{2+}$ inactivation

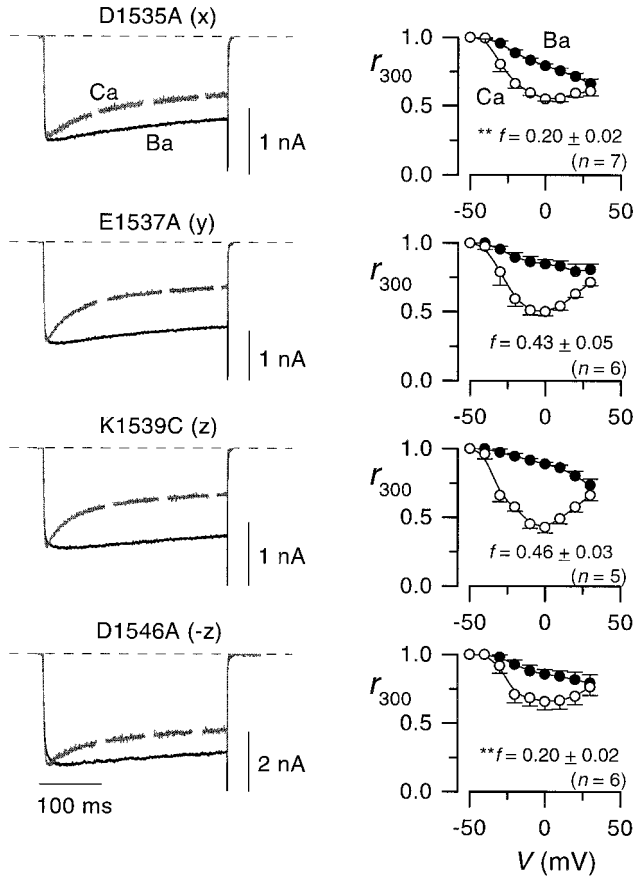


FIGURE 2 Alteration of residues thought to bind $Ca^{2+}$ have modest effects on $Ca^{2+}$-dependent inactivation. Residues corresponding to the *x*, *y*, *z*, and $-z$ positions of the consensus EF-hand were individually altered giving rise to the mutant channels D1535A, E1537A, K1539C, and D1546A, respectively. *Left:* exemplar $Ba^{2+}$ (*black*) and $Ca^{2+}$ (*gray*, *dashed*) currents elicited by depolarizing steps to 0 mV. *Right:* $r_{300}$ plots following the same format as in Fig. 1.

contained (in mM): 130 NMG-aspartate; 1 $MgCl_2$; 10 glucose; 10 4-aminopyridine; 10 HEPES (pH 7.4); and 10 $CaCl_2$ or 10 $BaCl_2$. Internal solution contained (in mM): 140 NMG-$MeSO_3$; 5 EGTA; 1 $MgCl_2$; 4 MgATP; and 10 HEPES (pH 7.3). Currents were low-pass filtered at 2 kHz, and digitally sampled at 10 kHz. Series resistance was typically <6 MΩ and was compensated by 70%. Repetition intervals were 30 s, holding potential ($V_H$) was −90 mV, and leak and capacitive transients were subtracted by a P/8 protocol.

## Mathematical modeling

Simulations in Fig. 6 were performed with MATLAB (MathWorks, Natick, MA), using the matrix exponential function (expm) to produce waveforms. Using least-squared error criteria, the simplex algorithm (fmins) was used to optimize fits to the $I_{norm}$-*V* relation between −50 and +40 mV, as well as to the $I_{norm}$ current waveforms at −30, 0, and +30 mV. All parameters were allowed to vary in the fit to the wild-type channel data in Fig. 6 *B*. The fit for V1548Y (Fig. 6 *C*) was subsequently obtained by holding fixed all rate constants, except those at the final opening step ($C_2 \leftrightarrow O_3$) and transduction step ($B_4 \leftrightarrow I_5$). Rate constants for the latter two transitions were then optimized with the simplex algorithm. The change in the C2 ↔ O3 rate constants was primarily necessitated by a leftward shift in the voltage required for half-activation of the V1548Y channel. Details of the model parameters are given in Table 1.

The experimental data that were fitted represent average channel behavior, processed so as to "isolate" the effects of $Ca^{2+}$-dependent inactivation from those of voltage-dependent inactivation. In each cell, $Ca^{2+}$-current waveforms elicited by 300-ms depolarizations were normalized to peak current elicited by voltage steps to +10 mV. These normalized currents were averaged across cells. To eliminate the small contribution of contaminating voltage-dependent inactivation upon these averages, an analogous averaging procedure was performed on $Ba^{2+}$ currents. For each step potential, the average of normalized $Ba^{2+}$ current was then used as a template to generate a smooth fit (exponential and offset) through the slowly decaying portion of the waveform. The smooth fit was then scaled in amplitude to have a value of unity at the time when the corresponding average of normalized $Ca^{2+}$ currents reached a peak. To obtain an $I_{norm}$ waveform that reflects "pure" $Ca^{2+}$-dependent inactivation, the average of normalized $Ca^{2+}$ currents was then divided through by the scaled fit, which reflects the influence of voltage-dependent inactivation. Such $I_{norm}$ waveforms, as illustrated by the gray traces on the left of panels *B* and *C* in Fig. 6, were used to compute average $r_{300}$-*V* and peak $I_{norm}$-*V* relations shown on the right.

The kinetic formulation in Fig. 6 *A* is not intended as a full-scale channel model. The scheme is only designed to predict coarse features of activation and $Ca^{2+}$ inactivation during depolarizing steps, but is inadequate to explain recovery from inactivation at hyperpolarized potentials. Because the present set of experiments is limited to data obtained during depolarizing steps, we have, for simplicity, omitted additional B and I states (Fig. 6 *A*) that would connect more directly with the closed $C_1$ and $C_2$ conformations, such as would be required to adequately represent recovery from inactivation. Moreover, to explain detailed kinetic properties of the channel, the number of steps representing the inactivation process and the number of closed states representing the activation pathway are likely to far exceed two. Finally, voltage-dependent inactivation is absent in the simple model. Though these additional features can be introduced into the core structure, the simple formulation here is optimal for the initial task of first-order testing against the basic set of data obtained in this study.

## Statistical analysis

The fraction of peak current remaining at the end of a 300-ms depolarization ($r_{300}$) as a function of voltage was used to quantitate the level of inactivation. The strength of $Ca^{2+}$-dependent inactivation was quantified by the parameter *f*, defined as the difference between $r_{300}$ values in $Ba^{2+}$ versus $Ca^{2+}$, taken at −10 mV. All data are presented as the mean ± SEM. Unpaired *t*-tests were used to compare *f* values between wild-type $Ca^{2+}$ channels ($\alpha_{1C}$ $\beta_{2a}$ $\alpha_2\delta$, in Fig. 1 *B*) and other constructs. The ** symbol denotes significance at $p < 0.001$, and * denotes significance at $p < 0.01$. Higher values of *p* were not considered to be statistically significant.

compared to wild-type channels (*panel B*), as characterized by reduced values of *f*, are denoted by the symbols ** ($p < 0.001$) and * ($p < 0.01$). For example, the reduction in $Ca^{2+}$ inactivation between panels *B* and *D* is statistically distinguished by the decreased in the mean *f* parameter, with significance at $p < 0.001$. The *f* value in panel *A* was 0.38 ± 0.04 ($n = 11$), and the *f* value in panel *C* was 0.03 ± 0.02 ($n = 15$, which is reduced significantly compared with panel *A*, $p < 0.001$). Population means in *A* and *B* include new data, supplemented with 6 and 5 cells, respectively, that were originally used in de Leon et al. (1995).

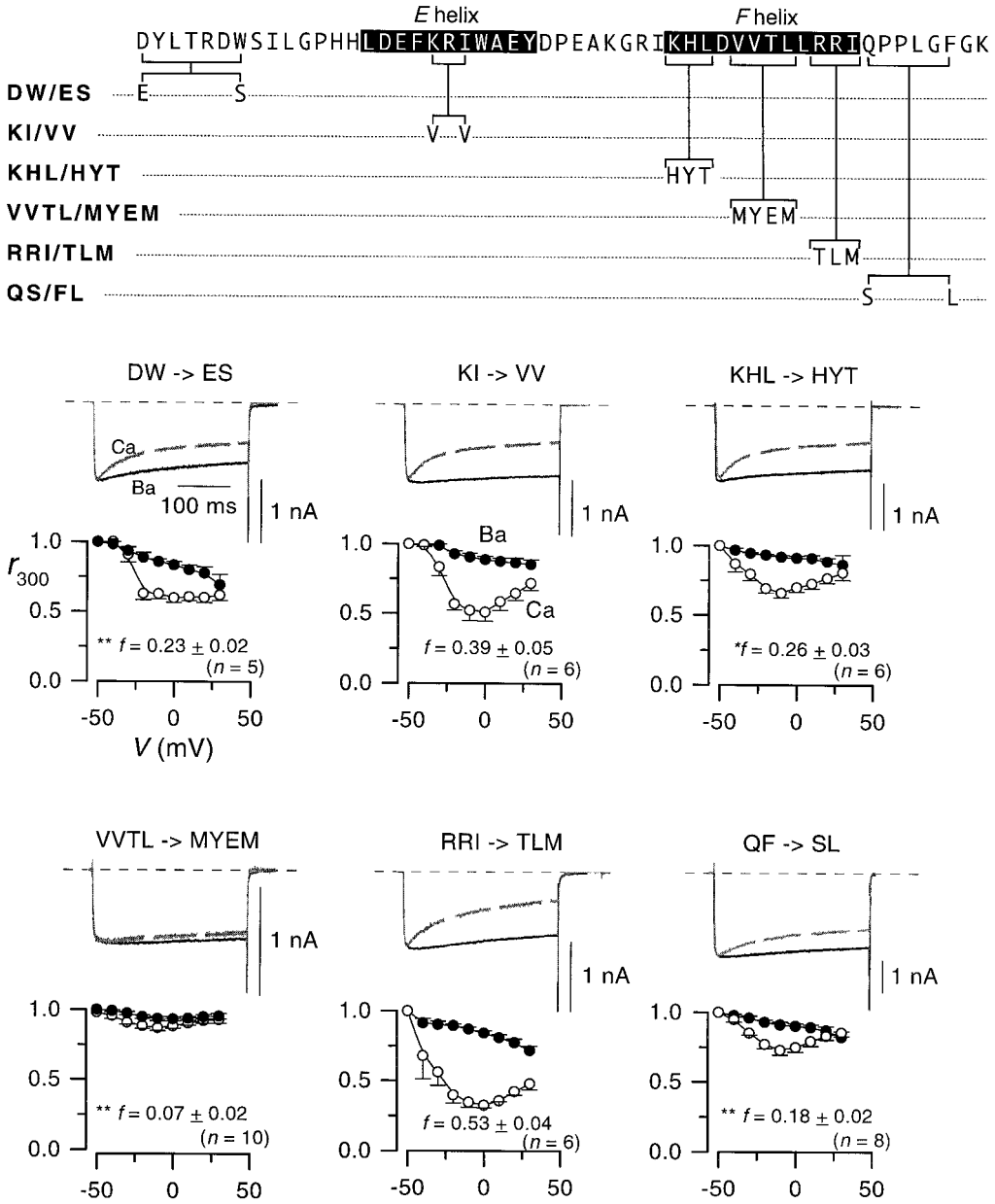


FIGURE 3 Localization of residues within the consensus EF-hand that are critical for $Ca^{2+}$-dependent inactivation. *Top:* the primary sequence of $\alpha_{1C}$ (amino acids 1510–1562) is shown with the *E* and *F* helices marked by shaded boxes. For each of the six mutant channels presented in this figure, from 2 to 4 amino acid residues were changed to their $\alpha_{1E}$ counterparts, as indicated beneath the primary sequence. *Bottom:* for each of the mutant channels, $r_{300}$ plots appear below exemplar $Ba^{2+}$ (*black*) and $Ca^{2+}$ (*gray*, *dashed*) currents that were elicited by depolarizations to 0 mV. The format of exemplar currents and $r_{300}$ summaries is identical to those in Fig. 1.

## RESULTS

### Confirmation that the $\alpha_{1C}$ consensus EF hand is essential for $Ca^{2+}$ inactivation

Fig. 1 (*A* and *B*) summarizes the $Ca^{2+}$ inactivation properties of wild-type L-type calcium channels, transiently expressed from cDNA clones in HEK 293 cells. In the original study of recombinant L-type channels from our lab (de Leon et al., 1995), $Ca^{2+}$ inactivation was characterized for channels composed of $\alpha_{1C}$ and $\beta_{2a}$ subunits, as illustrated in Fig. 1 *A*. Because L-type channels manifest distinct voltage- and $Ca^{2+}$-dependent inactivation mechanisms (Lee et al., 1985; Kass and Sanguinetti, 1984), the $\beta_{2a}$ subunit (Perez-Reyes et al., 1992) was chosen for coexpression with the main $\alpha_{1C}$ subunit, as the $\beta_{2a}$ subunit imparts the least voltage-dependent inactivation (Patil et al., 1998; Jones et al., 1998) in comparison to the other $\beta$ subunits (Perez-Reyes and Schneider, 1994). Accordingly, the slow decay of $Ba^{2+}$

**TABLE 1 Model parameters for $Ca^{2+}$ inactivation simulations in Fig. 6**

| Rate Constants | Value at $V_{half}$ | $V_{half}$ (mV) | $q$ (elementary charges) | $V_{reversal}$ (mV) |
|---|---|---|---|---|
| *Parameters for wild-type* | | | | |
| $k12$ ($ms^{-1}$) | 0.1341 | −28.20 | 1.70 | — |
| $k21$ ($ms^{-1}$) | 0.1670 | −28.20 | −1.70 | — |
| $k23$ ($ms^{-1}$) | 0.9635 | −10.85 | 1.11 | — |
| $k32$ ($ms^{-1}$) | 1.9000 | −10.85 | −1.11 | — |
| $k34$ ($ms^{-1}$ $mV^{-2}$) | $1.0476 \times 10^{-5}$ | — | 0 | 53.70 |
| $k43$ ($ms^{-1}$) | 2.7389 | — | 0 | — |
| $k45$ ($ms^{-1}$) | 2.2915 | — | 0 | — |
| $k54$ ($ms^{-1}$) | 0.0193 | — | 0 | — |
| *Parameters for V1548Y* | | | | |
| $k12$ ($ms^{-1}$) | 0.1341 | −28.20 | 1.70 | — |
| $k21$ ($ms^{-1}$) | 0.1670 | −28.20 | −1.70 | — |
| $k23$ ($ms^{-1}$) | 0.3661 | −10.85 | 1.11 | — |
| $k32$ ($ms^{-1}$) | 0.4597 | −10.85 | −1.11 | — |
| $k34$ ($ms^{-1}$ $mV^{-2}$) | $1.0476 \times 10^{-5}$ | — | 0 | 48.83 |
| $k43$ ($ms^{-1}$) | 2.7389 | — | 0 | |
| $k45$ ($ms^{-1}$) | 0.4660 | — | 0 | — |
| $k54$ ($ms^{-1}$) | 0.0123 | — | 0 | — |

Rate constants correspond to transitions diagramed in Fig. 6. Voltage-dependent rate constants ($k12$, $k21$, $k23$, $k32$) are of the form $k(V_{half}) \times \exp[q(V - V_{half})/(kT)]$. The complete rate constant for transitions from state 3 to state 4 is given by $k34 \times (V - V_{reversal})^2$. The $V - V_{reversal}$ term arises because $[Ca^{2+}]_{domain}$ drives the reaction, and $[Ca^{2+}]_{domain} \propto i \propto V - V_{reversal}$. The square term represents the binding of two $Ca^{2+}$ ions to CaM. In principle, $V_{reversal}$ should be the same between wild-type and V1548Y. The small change required for an optimal fit to V1548Y data probably reflects small variations in the quality of $Ca^{2+}$-current isolation near the reversal potential, between the groups of cells expressing wild-type and V1548Y channels. Predicted normalized currents, as plotted in Fig. 6, were calculated from probabilities as $I_{norm} = G_{norm}(V - V_{reversal})[P_{O3}(V) + P_{B4}(V)]$, where $G_{norm}$ was 0.0303 throughout. Predicted peak normalized currents and $r_{300}$ values were determined directly from simulated $I_{norm}$ waveforms. See Methods for details of numerical simulation and fits.

currents in Fig. 1 *A* (*black traces*) primarily reflects the sluggish time course of voltage-dependent inactivation, because the $Ca^{2+}$-inactivation mechanism is highly selective for $Ca^{2+}$ over $Ba^{2+}$ (Brehm and Eckert, 1978). By contrast, exemplar $Ca^{2+}$ currents at +0 mV decay by about half at the end of the depolarizing pulse (Fig. 1 *A*, *middle gray-dashed trace*), as expected from the robust induction of the $Ca^{2+}$-dependent inactivation process. Here and throughout, the $Ca^{2+}$ traces have been scaled upward to facilitate comparison of kinetics, and the fraction of peak current remaining at the end of 300-ms depolarizations ($r_{300}$) is plotted as a function of voltage (Fig. 1 *A*, *right*). Consistent with slow voltage-dependent inactivation, the $r_{300}$ relation with $Ba^{2+}$ declines only slightly and monotonically with increasing depolarization. In accord with hallmark behavior of $Ca^{2+}$ inactivation, the corresponding $r_{300}$ relation with $Ca^{2+}$ exhibits a characteristic U-shape, as expected of inactivation driven by $Ca^{2+}$ entry rather than voltage. A direct measure of the extent of $Ca^{2+}$ inactivation is therefore provided by the difference between the $r_{300}$ plots in $Ba^{2+}$ and $Ca^{2+}$, with the difference at −10 mV given by the parameter $f$.

In Fig. 1 *B*, the $\alpha_2\delta$ subunit was coexpressed with $\alpha_{1C}$ and $\beta_{2a}$ to approximate more closely the heteromultimeric structure of native channels (De Waard et al., 1996; Walker and De Waard, 1998). Interestingly, inclusion of the $\alpha_2\delta$ subunit resulted in more robust $Ca^{2+}$ inactivation, as illustrated by the more rapid decay of specimen $Ca^{2+}$ current at +0 mV in comparison to that observed in cells expressing $\alpha_{1C}$ and $\beta_{2a}$ alone (compare Fig. 1, *A* and *B*). There is also a slight enhancement of voltage-dependent inactivation as observed by others (Ferreira et al., 1997), but this is still small by comparison to $Ca^{2+}$ inactivation. Hence, in this study coexpression with the $\alpha_2\delta$ subunit was used to increase the sensitivity of our subsequent screen for mutants that affect $Ca^{2+}$ inactivation.

The effect of the $\alpha_2\delta$ subunit to enhance $Ca^{2+}$ inactivation may help to explain some, but not all, of the controversy regarding the importance of the consensus EF hand. Previously, we identified a 53-amino acid segment near the beginning of the $\alpha_{1C}$ CI region that was critical for $Ca^{2+}$ inactivation (Fig. 1, *top*) (de Leon et al., 1995). The extent of the consensus EF hand is defined by the lateral margins of the highlighted *E* and *F* helices. When this segment of $\alpha_{1C}$ was replaced by the analogous segment from the $\alpha_{1E}$ isoform (which lacks $Ca^{2+}$ inactivation), the resulting chimera ($\alpha_{1CE\text{-}3}$) exhibited no appreciable $Ca^{2+}$-dependent inactivation when coexpressed with $\beta_{2a}$ alone (de Leon et al., 1995), a result that we confirmed extensively in Fig. 1 *C*. However, when $\alpha_{1CE\text{-}3}$ was coexpressed with $\beta_{2a}$ and $\alpha_2\delta$ subunits, a small but statistically resolved amount of $Ca^{2+}$ inactivation ($f = 0.04$) was observed in averaged data. Nonetheless, there was still an enormous reduction of $Ca^{2+}$ inactivation relative to wild-type channels (compare Fig. 1, *B* and *D*), which emphasizes the essential nature of the consensus EF hand to $Ca^{2+}$ inactivation. We therefore proceeded to map the structural basis for the virtual knockout of $Ca^{2+}$ inactivation.

## The $\alpha_{1C}$ consensus EF hand may not bind $Ca^{2+}$ according to a classic EF-hand mechanism

In an earlier report from our lab (de Leon et al., 1995), the simplest hypothesis was suggested to explain the functional reduction of $Ca^{2+}$ inactivation by swapping EF-hand regions (Fig. 1, *B* and *D*): the $\alpha_{1C}$ consensus EF hand is capable of binding $Ca^{2+}$ and serving as the $Ca^{2+}$ sensor for $Ca^{2+}$ inactivation, while the homologous region in $\alpha_{1E}$ binds $Ca^{2+}$ far less well. Many EF hand-containing proteins such as calmodulin, troponin C, and recoverin have been studied at the atomic level by x-ray crystallography and nuclear magnetic resonance (Falke et al., 1994). These studies indicate that EF hands form a helix-loop-helix structure, where the $Ca^{2+}$ ion is typically coordinated by six amino acids (designated $x$, $y$, $z$, $-y$, $-x$, and $-z$) that lie mostly within the loop bracketed by *E* and *F* helices of this motif (Fig. 1, *top*). If $Ca^{2+}$ binding to the consensus EF

hand in $\alpha_{1C}$ initiates the conformational changes that lead to inactivation, it should be possible to disrupt $Ca^{2+}$ inactivation by altering the amino acid residues thought to bind $Ca^{2+}$.

To test this hypothesis, we used site-directed mutagenesis to individually alter the amino acids located at the *x*, *y*, *z*, and $-z$ coordinates of the consensus EF hand in the $\alpha_{1C}$ channels (see Fig. 1, *top*, and Methods). Fig. 2 summarizes the $Ca^{2+}$-inactivation properties of these mutant $\alpha_{1C}$ channels. For each mutant, exemplar $Ba^{2+}$ and $Ca^{2+}$ currents at +0 mV are shown at left, and averaged $r_{300}$ data at right. Mutations at two of the positions, E1537A (*y*) and K1539C (*z*), failed to alter $Ca^{2+}$ inactivation significantly compared with control (Fig. 1 *B*). Alterations at the other two positions, D1535A (*x*) and D1546A ($-z$), did reduce $Ca^{2+}$ inactivation by about half, as demonstrated by statistically resolved changes in the parameter *f*. However, none of these alterations came close to eliminating $Ca^{2+}$ inactivation, fitting poorly with the general trend that such mutations reduce the $Ca^{2+}$ affinity of classic EF hands by 10–1000 fold (Linse and Forsen, 1995). Our data here agree with the results of similar experiments performed by other groups (Zhou et al., 1997; Bernatchez et al., 1998), and point to one of two conclusions. First, if the $\alpha_{1C}$ consensus EF hand does bind $Ca^{2+}$ as in classic EF-hand proteins, then such $Ca^{2+}$ binding is not strongly linked to channel inactivation. Alternatively, if the EF hand serves as an important $Ca^{2+}$ sensor for inactivation, then it must bind $Ca^{2+}$ in an unorthodox and previously unreported fashion, unlike that of classic EF-hand proteins. Thus, it seemed unlikely that the consensus EF hand functions as the $Ca^{2+}$ sensor for inactivation.

## $Ca^{2+}$ inactivation depends critically on residues in the *F* helix of the consensus EF hand

Regardless of its ability to bind $Ca^{2+}$, the consensus EF hand of the $\alpha_{1C}$ channel is still a crucial domain for $Ca^{2+}$ inactivation (Fig. 1, *B* and *D*). We therefore screened all remaining differences between $\alpha_{1C}$ and $\alpha_{1E}$ in the 53-amino acid segment that was exchanged in the chimera $\alpha_{1CE\text{-}3}$ (Fig. 1). Starting with wild-type $\alpha_{1C}$, amino acid residues that differ between $\alpha_{1C}$ and $\alpha_{1E}$ have been changed in clusters, such that each mutant channel contains substitutions of 2–4 amino acids (Fig. 3, *top*). The $Ca^{2+}$ inactivation properties for each of these mutants is summarized in Fig. 3, with exemplar $Ba^{2+}$ and $Ca^{2+}$ traces shown at the top, and averaged $r_{300}$ data at the bottom. Some of the mutants exhibited $Ca^{2+}$ inactivation that was statistically indistinguishable from wild type (KI → VV and RRI → TLM). Interestingly, the KHL → HYT mutations include a change in the lysine residue at the $-x$ position of the consensus EF hand, and these mutations decreased $Ca^{2+}$ inactivation by over a third. The reduction of inactivation was stronger in DW → ES and QF → SL channels, where $Ca^{2+}$ inactivation was approximately halved. Most strikingly, $Ca^{2+}$ inactivation was almost completely lost in VVTL → MYEM channels, with no statistically resolved difference from the $\alpha_{1CE\text{-}3}$ chimera (mean *f* values of 0.07 and 0.04, respectively). Hence, changes in just four amino acids in the *F* helix (VVTL → MYEM) account for most, if not all, of the functional effect in the chimeric channel $\alpha_{1CE\text{-}3}$.

To identify the single amino acid that is most critical to $Ca^{2+}$ inactivation in this four-residue segment (VVTL), each amino acid was exchanged individually, giving rise to the mutants V1547M, V1548Y, T1549E, and L1550M (Fig. 4). Two of the mutant channels (T1549E, L1550M) showed $Ca^{2+}$ inactivation that was statistically indistinguishable from wild type. By contrast, $Ca^{2+}$ inactivation was almost

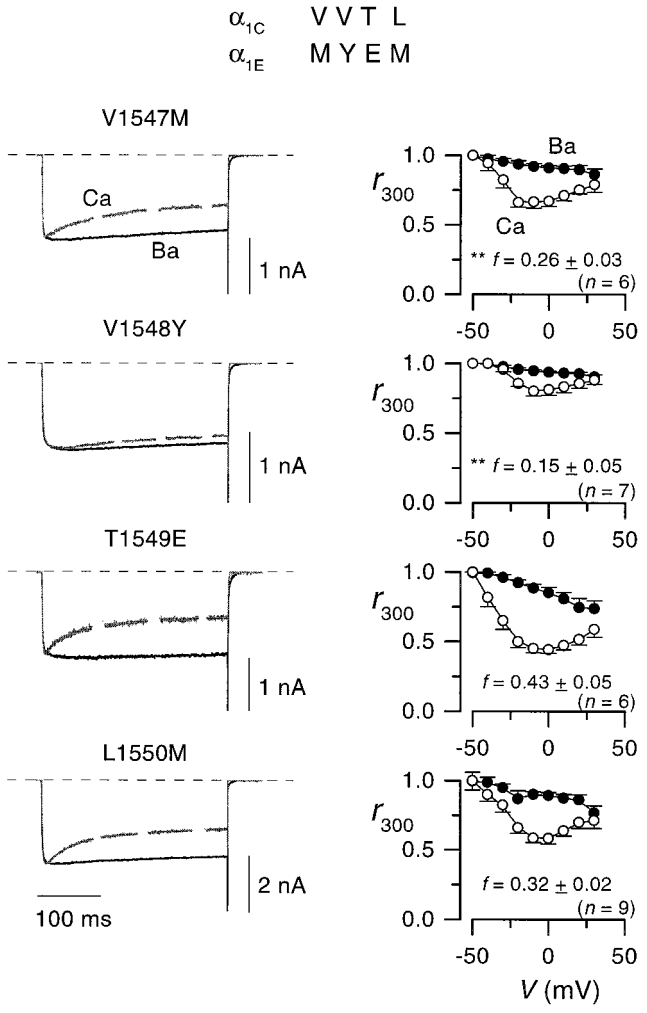


FIGURE 4 The amino acids that comprise the VVTL motif in $\alpha_{1C}$ were changed individually to their $\alpha_{1E}$ counterparts. *Left:* exemplar $Ba^{2+}$ (*black*) and $Ca^{2+}$ (*gray*, *dashed*) currents elicited from step depolarizations to 0 mV. *Right:* corresponding $r_{300}$ plots. The format of exemplar currents and $r_{300}$ summaries is identical to those in Fig. 1. Most of the knockout of $Ca^{2+}$ inactivation produced by the VVTL → MYEM cluster mutation is reproduced by the V1548Y point mutation.

halved in V1547M channels, and the single exchange of tyrosine for valine in V1548Y channels accounts for much of the virtual ablation of $Ca^{2+}$ inactivation seen in VVTL → MYEM channels.

## DISCUSSION

Although CaM is the dominant $Ca^{2+}$ sensor for $Ca^{2+}$ inactivation of L-type channels (Peterson et al., 1999; Zuhlke et al., 1999; Qin et al., 1999), this study unequivocally underscores the critical nature of the $\alpha_{1C}$ consensus EF hand to the inactivation process. In agreement with previous work from our lab (de Leon et al., 1995), we here confirmed the essential knockout of $Ca^{2+}$ inactivation in the chimeric channel $\alpha_{1CE\text{-}3}$, in which a 53-residue segment of $\alpha_{1C}$ that contains the EF hand was replaced by the analogous segment from a non-inactivating $\alpha_{1E}$ channel. Systematic mutagenesis of this 53-residue stretch in $\alpha_{1C}$ further revealed that a four-amino acid cluster (VVTL) within the *F* helix of the EF-hand motif is itself critical for $Ca^{2+}$ inactivation, and much of the essential chemistry resides in the second valine. Mutations of presumed $Ca^{2+}$-coordinating residues in the consensus EF hand produced only ~2-fold reduction of $Ca^{2+}$ inactivation, making it appear unlikely that the EF hand serves as a significant $Ca^{2+}$ sensor for channel inactivation. Our findings have implications for previously reported results, the physiological potential for $Ca^{2+}$ binding to the consensus EF hand, and the possible mechanistic interrelation between CaM and the EF-hand motif, as discussed below.

### Relation to previous studies

The effect of the $\alpha_2\delta$ subunit to enhance $Ca^{2+}$ inactivation (Fig. 1) helps to explain some, but not all, of the differing results concerning the importance of the consensus EF hand for $Ca^{2+}$ inactivation. Although our chimera $\alpha_{1CE\text{-}3}$ exhibited no appreciable $Ca^{2+}$ inactivation when coexpressed with $\beta_{2a}$ alone (Fig. 1 *C*) (as in de Leon et al. (1995)), addition of the $\alpha_2\delta$ subunits revealed a small but statistically resolved amount of $Ca^{2+}$ inactivation (Fig. 1 *D*). Even so, there was still a virtual knockout of $Ca^{2+}$ inactivation relative to wild-type channels (compare Fig. 1, *B* and *D*), which stands in contrast to the results of Zhou et al. (1997). Using the *Xenopus* oocyte expression system, they reported substantial $Ca^{2+}$ inactivation in a chimeric channel (EC61) that is similar to our $\alpha_{1CE\text{-}3}$ chimera, in which a 53-amino-acid stretch containing the consensus EF hand of $\alpha_{1C}$ has been replaced with homologous $\alpha_{1E}$ sequence (Fig. 1). Although only the $\beta_{2a}$ subunit was specifically coexpressed with EC61 (Zhou et al., 1997), *Xenopus* oocytes do contain high levels of endogenous $\alpha_2\delta$ subunits (Singer-Lahat et al., 1992), so the slight enhancement of $Ca^{2+}$ inactivation observed here by cotransfection of $\alpha_2\delta$ subunits in HEK 293 cells helps to explain some of the difference between results reported for expression in HEK 293 cells (de Leon et al., 1995) and oocytes (Zhou et al., 1997). However, close inspection of the exemplar traces in Zhou et al. (1997) reveals that $Ca^{2+}$ inactivation, though substantially reduced compared to wild-type $\alpha_{1C}$, is clearly more prominent than in our results, even with coexpression of the $\alpha_2\delta$ subunit in HEK 293 cells.

To explore the possibility that a subtle difference in cDNA constructs could account for the contrasting results, we have also characterized the $Ca^{2+}$ inactivation properties of a construct that is strictly comparable to EC61 at the amino acid level, in that only the 29-amino acid, EF-hand region of $\alpha_{1E}$ has been substituted into $\alpha_{1C}$. Fig. 5 summarizes the inactivation properties of this construct ($\alpha_{1CE\text{-}3/QF/DW}$) when coexpressed in HEK 293 cells with $\beta_{2a}$ and $\alpha_2\delta$ subunits. Though not quite statistically resolved, the mean behavior of $\alpha_{1CE\text{-}3/QF/DW}$ channels (Fig. 5) hints that $Ca^{2+}$ inactivation is somewhat stronger than for $\alpha_{1CE\text{-}3}$ channels (Fig. 1 *D*), with *f* values of 0.08 ± 0.03 ($n = 6$) versus 0.04 ± 0.03 ($n = 6$), respectively. Nonetheless, the strength of $Ca^{2+}$ inactivation for $\alpha_{1CE\text{-}3/QF/DW}$ channels was still very weak, and there remains a substantial difference between the results reported by Zhou et al. (1997) and those we have presented here and before (de Leon et al., 1995).

Zuhlke and Reuter (1998) provide a different perspective on the importance of the consensus EF hand. They find that simple deletion of the EF-hand motif from $\alpha_{1C}$ abolishes $Ca^{2+}$ inactivation, in agreement with the implications of our

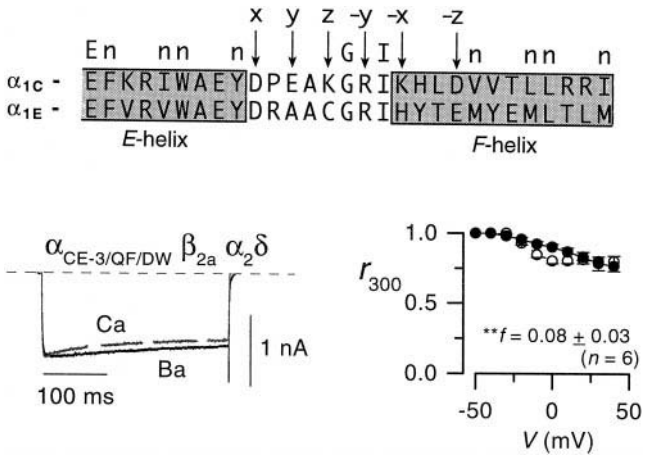


FIGURE 5 Marked attenuation of $Ca^{2+}$-dependent inactivation in a chimeric $Ca^{2+}$ channel $\alpha_{1CE\text{-}3/QF/DW}$, corresponding to an $\alpha_{1C}$ channel in which only the 29 amino acids comprising the canonical EF-hand motif have been replaced by their $\alpha_{1E}$ counterparts. *Top:* alignment of $\alpha_{1C}$ and $\alpha_{1E}$ regions that are swapped in chimeric channel $\alpha_{1CE\text{-}3/QF/DW}$. Amino acids 1526–1554 of $\alpha_{1C}$ are shown, corresponding to the strict extent of the 29-amino-acid, canonical EF hand. *Bottom, left:* exemplar $Ba^{2+}$ (*black*) and $Ca^{2+}$ (*gray*, *dashed*) currents elicited by step depolarizations to +0 mV. *Bottom, right:* corresponding $r_{300}$ plots, averaged from 6 cells, with the $Ba^{2+}$ data plotted as solid circles. The format of exemplar currents and $r_{300}$ summaries are identical to those in Fig. 1.

mutagenesis and chimeric channel analyses. Zhou et al. (1997) made a similar deletion construct, but were unable to express functional channels.

With regard to voltage-dependent inactivation, our results echo the growing consensus that structural determinants for both $Ca^{2+}$- and voltage-dependent inactivation appear to be interlaced along the $\alpha_{1C}$ carboxyl tail (Zhang et al., 1994; Klockner et al., 1995; Soldatov et al., 1997). Some of our EF-hand mutations affect the decay of $Ba^{2+}$ current, which presumably reflects properties of voltage-dependent inactivation (but see Ferreira et al., 1997). A particularly obvious example comes with mutation at the *x* coordinate of the consensus EF hand (D1535A, Fig. 2), which induces marked acceleration in the decay of $Ba^{2+}$ currents.

Finally, although this study has focused on the $\alpha_{1C}$ CI region in general and the consensus EF hand in particular, it should be mentioned that other regions have been suggested as additional structural mediators of $Ca^{2+}$-dependent modulation of channel gating. Portions of the $\alpha_{1C}$ carboxyl tail that are distal to the CI region, as well as I–II and II–III interdomain linkers, have been proposed to be important for $Ca^{2+}$ inactivation (Adams and Tanabe, 1997). The potential contribution of the distal $\alpha_{1C}$ carboxyl tail seems all the more plausible, given the recent discovery of $Ca^{2+}$-dependent facilitation and inactivation of P/Q-type calcium channels that involves CaM binding to a "CBD" domain located distally on the $\alpha_{1A}$ carboxyl tail (Lee et al., 1999). However, with regard to the distal $\alpha_{1C}$ carboxyl tail, the impact on $Ca^{2+}$ inactivation seems limited to a modulatory rather than essential role, as we have previously observed that $Ca^{2+}$ inactivation appears largely unchanged upon truncation of such distal regions (de Leon et al., 1995). Furthermore, whatever role the interdomain linkers play in $Ca^{2+}$ inactivation, it must be conserved across different channel types, as donation of the $\alpha_{1C}$ carboxyl tail confers $Ca^{2+}$ inactivation to backbones for $\alpha_{1E}$ (de Leon et al., 1995; Peterson et al., 1999) and $\alpha_{1A}$ (D. T. Yue and J. G. Mulle, unpublished results).

## Does the consensus EF hand engage in physiological $Ca^{2+}$ binding?

The results of mutations on presumed $Ca^{2+}$-coordinating residues in the consensus EF hand square poorly with a scenario in which the EF hand represents a significant $Ca^{2+}$ sensor for inactivation while binding $Ca^{2+}$ according to a classic EF-hand mechanism (Fig. 2) (Zhou et al., 1997; Bernatchez et al., 1998). However, these results in themselves do not exclude $Ca^{2+}$ binding to the consensus EF hand under physiological conditions. First, it is possible that $Ca^{2+}$ does bind to the EF hand in a classic manner, but that such binding is not tightly linked to channel inactivation. Alternatively, the EF hand could still provide an important $Ca^{2+}$-sensing function for inactivation, given the presumed proximity of the consensus EF hand to the inner mouth of the channel pore. In this region, $Ca^{2+}$ diffusion modeling (Simon and Llinas, 1985) would predict that the $Ca^{2+}$ concentrations presented to the EF-hand domain could extend toward the millimolar range, far higher than presented to conventional EF-hand proteins. To accommodate such unusual performance criteria, the consensus EF hand may be designed to coordinate $Ca^{2+}$ in a fashion that differs considerably from that in conventional EF-hand proteins. Otherwise, the consensus EF hand might be immediately "blinded" by the enormous $Ca^{2+}$ signal emanating from the very first opening of the channel. In fact, preliminary biophysical studies of peptides encoding the consensus EF hand indicate $Ca^{2+}$ binding in the 10–50 $\mu$M range (Villain et al., 1999). However, any such $Ca^{2+}$ binding would be unlikely to serve as the primary $Ca^{2+}$-sensing event for inactivation, as we showed essentially *complete* ablation of $Ca^{2+}$ inactivation upon overexpression of mutant CaMs lacking appreciable $Ca^{2+}$ binding (Peterson et al., 1999). Nonetheless, low-affinity $Ca^{2+}$ binding to the consensus EF hand could still serve to modulate the efficacy of the primary $Ca^{2+}$-sensing mechanism carried by CaM.

The high $Ca^{2+}$ concentration environment near the inner mouth of the channel also raises a paradox in connection with the role of CaM as $Ca^{2+}$ sensor for inactivation, as follows. Because CaM interacts with the IQ-like motif, we also presume that CaM is situated near the inner channel mouth. Given that the C-terminal domain of CaM appears to be the relevant $Ca^{2+}$-sensing domain for channel inactivation (Peterson et al., 1999), and that $Ca^{2+}$ may have submicromolar affinity for this domain (Falke et al., 1994), it remains challenging to understand how CaM can mediate smoothly graded changes in the extent of $Ca^{2+}$ inactivation that vary with the rate of $Ca^{2+}$ entry.

## Proposed mechanistic interrelationship between CaM and the consensus EF hand

How do CaM, the IQ-like motif, and the consensus EF hand interrelate within the context of an overall molecular mechanism of $Ca^{2+}$ inactivation? Although it is premature to draw firm conclusions, the identification of major pieces in the puzzle make it possible to raise a working hypothesis.

An intriguing aspect of our results is that the primary molecular determinant within the consensus EF hand turns out to be a hydrophobic patch in the *F* helix (VVTL). In structural models of the conformational changes induced by $Ca^{2+}$ binding to EF-hand proteins, such hydrophobic patches figure prominently in transducing $Ca^{2+}$ binding into functional sequelae. According to the classic HMJ model (Herzberg et al., 1986) and its subsequent refinements (Chazin, 1995), hydrophobic residues in *E* and *F* helices tend to interact with each other in apo EF hands, but become exposed to the outside world subsequent to large changes in interhelical angles induced by $Ca^{2+}$ binding. The exposed hydrophobic patches then interact with target surfaces, and

thereby modulate effector molecules. Perhaps, hydrophobic patches in the helices of the $\alpha_{1C}$ consensus EF hand (e.g., VVTL) serve such a transduction function, somehow linking $Ca^{2+}$ binding to channel inactivation.

The problem with such a proposal is that $Ca^{2+}$ binding to CaM, rather than the consensus EF hand, serves as the primary initiatory event for inactivation. A possible solution comes from extensive studies of recoverin (Flaherty et al., 1993; Zozulya and Stryer, 1992; Ames et al., 1997; Tanaka et al., 1995), a $Ca^{2+}$ sensor involved in vision that contains four EF-hand motifs (EF-1 and EF-2 in one pair, EF-3 and EF-4 in a second). Of particular relevance is the fact that although EF-1 does not bind $Ca^{2+}$, $Ca^{2+}$ binding to EF-2 ultimately induces a large conformational change in EF-1, which in turn ejects a buried myristoyl group. Exposure of the latter group results in translocation of recoverin from the cytosol to the membrane. The analogy for L-type channels could be that the consensus EF hand acts like EF-1, and CaM like EF-2. $Ca^{2+}$ binding to CaM would then induce conformational changes in the consensus EF hand, leading to exposure of its helical hydrophobic patches, and interaction of these patches with target regions on the channel would bring about inactivation. The only variation required for the L-type channel is that the coupling between CaM and the consensus EF hand must occur in trans across molecules, but this seems plausible given that CaM may be constitutively tethered to the channel like an integral subunit (Peterson et al., 1999).

As a first step in testing such a working hypothesis, we asked whether the proposed transduction role for the consensus EF hand is compatible with the detailed $Ca^{2+}$ inactivation properties of wild-type and mutant V1548Y channels. Although numerous kinetic models of $Ca^{2+}$ inactivation have been developed (e.g., Standen and Stanfield, 1982; Sherman et al., 1990; Shirokov et al., 1993; Noceti et al., 1998), none have incorporated key elements of our working hypothesis, such as separate steps for $Ca^{2+}$ binding and subsequent transduction into channel inactivation, and multivalent $Ca^{2+}$ binding of CaM. To evaluate the quantitative feasibility of our working hypothesis, we therefore developed the simplest form of a kinetic mechanism incorporating these key features (Fig. 6 *A*).

The core attributes of this kinetic formulation are as follows. The activation pathway describing outward movement of S4 voltage sensors (Yang and Horn, 1996; Larsson et al., 1996) and opening of a cytoplasmic gate (Liu et al., 1997; Perozo et al., 1999) is minimally represented by two closed ($C_1$, $C_2$) and one open ($O_3$) conformation(s) (Imredy and Yue, 1994), linked by voltage-dependent transitions.

As in more recent models of $Ca^{2+}$ inactivation (Sherman et al., 1990; Shirokov et al., 1993; Noceti et al., 1998), we adopt a "local $Ca^{2+}$ domain" approximation, in which 1) the $Ca^{2+}$ responsible for inactivation is situated within ~100 Å of the inner channel pore, and 2) $Ca^{2+}$ influx through an individual channel is solely responsible for driving its own inactivation. The first part of the local domain approximation is easily justified based on the apparent proximity of the IQ-like motif to the channel pore, and on the insensitivity of $Ca^{2+}$ inactivation to intracellular dialysis with even fast chelators of $Ca^{2+}$ (BAPTA) (Noceti et al., 1998; Deisseroth et al., 1996). The second part is not strictly true (Imredy and Yue, 1992); however, it seems a reasonable simplification in HEK 293 cells, because the strength of $Ca^{2+}$ inactivation grows only slightly with large increases in channel expression (Fig. 2 *C* in Peterson et al. (1999)). Under the local domain approximation, the $Ca^{2+}$ concentration that drives tethered CaM ($[Ca^{2+}]_{domain}$) would be virtually synchronized in time with single-channel openings, and directly proportional to the unitary current $i$ (Sherman et al., 1990), such that $[Ca^{2+}]_{domain} \propto i$ (when the channel is open) or 0 (when it is closed or inactivated).

In the local domain case, then, we need only consider $Ca^{2+}$ binding to CaM when the channel is in the open state ($O_3$). For computational simplicity we combine $Ca^{2+}$ binding to CaM and its subsequent interaction with the IQ-like domain into a single transition, yielding a CaM-bound form of the channel ($B_4$). This channel conformation still conducts current. Only after CaM is bound does the channel undergo a subsequent conformational change to reach a non-conducting, inactivated state ($I_5$). This transduction step could correspond to CaM-induced, full opening of the consensus EF hand, and ensuing strong interaction of target regions with exposed helical hydrophobic stretches. This strong interaction is schematized as a thick dashed curve in Fig. 6 *A*, symbolizing stabilization of a cytoplasmic activation gate (Liu et al., 1997; Perozo et al., 1999) in the closed position (Imredy and Yue, 1994). Before full opening of the consensus EF hand induced by CaM, the EF hand is presumed to adopt a relatively closed conformation, in which helical hydrophobic patches interact only weakly (or differently) with the cytoplasmic gate, in a manner that permits ready channel opening. This form of interaction is represented as a thin, dashed curve in Fig. 6 *A*.

The transitions among $O_3$, $B_4$, and $I_5$ states merit special attention. Because the molecular events underlying these transitions probably occur outside the membrane electric field, the corresponding rate constants are considered voltage independent. Finally, to incorporate multivalent $Ca^{2+}$ binding of CaM, we considered our previous result that $Ca^{2+}$ binding to only the C-terminal lobe of CaM (with two $Ca^{2+}$ binding sites) appears to be important for inactivation (Peterson et al., 1999). Hence, the rate constant pertaining to $O_3 \rightarrow B_4$ is set proportional to $[Ca^{2+}]^2_{domain}$, in accord with two possible scenarios of dual $Ca^{2+}$ binding to CaM followed by CaM-$Ca_2$ binding to the IQ domain ($O_3 \leftrightarrow O_3Ca_2 \leftrightarrow B_4$). These scenarios lend themselves to the computationally simple outcome that the $O_3 \rightarrow B_4$ rate constant is proportional to $[Ca^{2+}]^2_{domain}$. One case is that $Ca^{2+}$ (un)binding to CaM ($O_3 \leftrightarrow O_3Ca_2$) is rate-limiting relative to (un)binding to the IQ domain ($O_3Ca_2 \leftrightarrow B_4$), and that two $Ca^{2+}$ ions (un)bind simultaneously to CaM. This case coin-

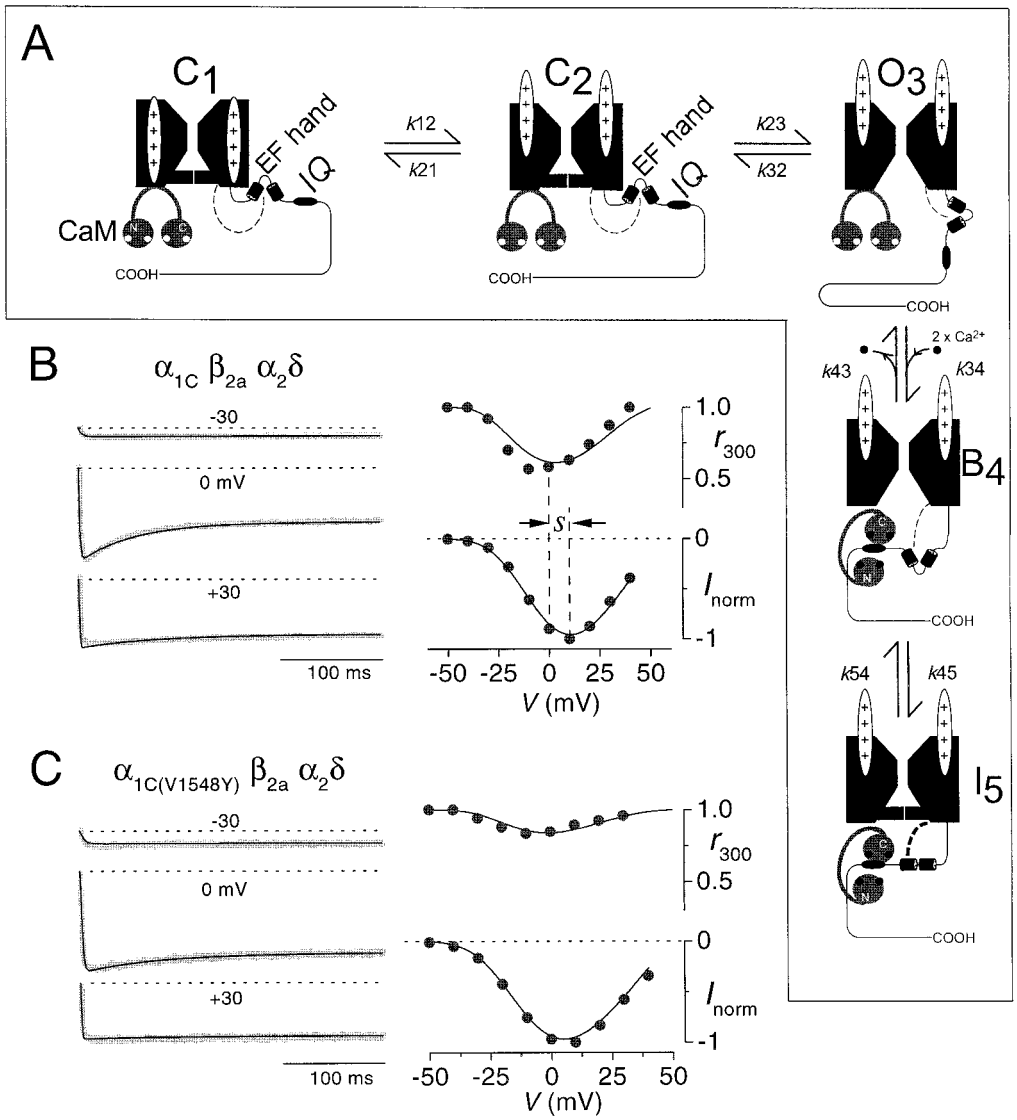


FIGURE 6 Proposed mechanism of $Ca^{2+}$-dependent inactivation, in which calmodulin serves as $Ca^{2+}$ sensor for inactivation, and the consensus EF hand serves in subsequent transduction steps that translate calmodulin binding into channel inactivation. (*A*) Five-state kinetic scheme used to model calcium-channel activation and $Ca^{2+}$-dependent inactivation. Depolarization causes the voltage sensors (ellipses with "+" charges) to move outward as the channel traverses closed states ($C_1$, $C_2$) toward the channel open state ($O_3$). Opening is viewed as rearrangement of a cytoplasmic gate, which is permitted by the outward disposition of voltage sensors. $Ca^{2+}$ entering through the channel binds to the tethered calmodulin (CaM, *dumbbell shape*), which in turn binds to the IQ motif located downstream of the EF-hand ($B_4$). State $B_4$ still conducts $Ca^{2+}$ current, as channel inactivation requires a subsequent conformational change of the consensus EF hand that stabilizes (*thick dashed curve*) the closed position of the cytoplasmic gate ($I_5$). Before this conformational change, the EF hand is proposed to interact weakly (or differently) with the cytoplasmic gate (*thin dashed line*), in a manner that permits ready opening of the gate. Although CaM binds four $Ca^{2+}$ ions in the transition between $O_3$ and $B_4$, our previous work (Peterson et al., 1999) suggests that $Ca^{2+}$ binding to only the C-terminus of CaM (with 2 $Ca^{2+}$ sites) is critical for $Ca^{2+}$ inactivation. Hence, within the context of $Ca^{2+}$ inactivation, the relevant stoichiometry of $Ca^{2+}$ binding is two, as marked near the *k*34 step. In addition, to signify the apparently non-essential role of $Ca^{2+}$ binding to the N-terminal domain of CaM in mediating channel inactivation, the N-terminal domain of CaM is "retracted" somewhat from the IQ domain in states $B_4$ and $I_5$. (*B*) Comparison of averaged wild-type channel ($\alpha_{1C}$ $\beta_{2a}$ $\alpha_2\delta$) properties (*gray traces* and *symbols*, averaged from 6 cells) and model simulations (*smooth curves*, generated by the model in *A* with parameters given in Table 1). *Left:* $Ca^{2+}$-current waveforms during depolarizations to the indicated potentials. Amplitudes have been normalized to peak current amplitude at +10 mV, and the scale is given by the *y* axis of the $I_{norm}$-*V* relation shown at right. *Right:* $r_{300}$ and peak normalized $Ca^{2+}$ current ($I_{norm}$), plotted as a function of voltage (*V*). The leftward shift observed in the minimum of the $r_{300}$-*V* plot with respect to the peak $I_{norm}$-*V* relation is designated with by the parameter *s*. (*C*) Comparison of averaged mutant channel ($\alpha_{1C(V1548Y)}$ $\beta_{2a}$ $\alpha_2\delta$) properties (*gray traces* and *symbols*, averaged from 7 cells) and model simulations (*smooth curves*, generated by the model in *A* with parameters given in Table 1). Format as in *B*. Consistent with a transduction role for the consensus EF-hand region, fits to the mutant data only required significant changes to the rate constants between $B_4$ and $I_5$, and between $C_2$ and $O_3$. Other parameters were essentially identical to those for the wild-type channel in *B*.

cides exactly with our simplified representation. The other case is that CaM (un)binding to the IQ domain ($O_3Ca_2 \leftrightarrow B_4$) is rate-limiting relative to $Ca^{2+}$ (un)binding to CaM ($O_3 \leftrightarrow O_3Ca_2$), and that two $Ca^{2+}$ ions (un)bind to CaM in a highly cooperative manner described in the steady state by a Hill equation. This case also reduces to a lumped, two-state representation ($O_3 \leftrightarrow B_4$), but here the $O_3 \rightarrow B_4$ rate constant is proportional to $[Ca^{2+}]^2_{domain}/(K^2_{half} + [Ca^{2+}]^2_{domain})$, where $K_{half}$ is the $[Ca^{2+}]_{domain}$ required to half-saturate the $O_3 \leftrightarrow O_3Ca_2$ reaction. The latter term reduces to $[Ca^{2+}]^2_{domain}$ when $[Ca^{2+}]_{domain} \ll K_{half}$, a condition that is partially satisfied because the maximal steady-state $Ca^{2+}$ inactivation that we model is ~50% (Fig. 6 *B*). Because CaM is probably tethered constitutively to the channel complex (Peterson et al., 1999), there is uncertainty about the detailed reaction kinetics of the relevant CaM, as such tethering could well alter kinetic properties via allosteric interactions. In the absence of reliable kinetic data for the relevant CaM, we have implemented the computationally simple $O_3 \leftrightarrow B_4$ representation, with the $O_3 \rightarrow B_4$ rate constant proportional $[Ca^{2+}]^2_{domain}$. This approximation suffices to illustrate some of the behaviors that may arise from multivalent $Ca^{2+}$ binding to CaM, but will likely be subject to revision with regard to quantitative details. Finally, in this version, no $Ca^{2+}$ binding to the consensus EF hand is represented in the $B_4 \leftrightarrow I_5$ step. Details of the model formulation are described in Table 1 and the Methods.

Fig. 6 *B* compares quantitative fits of the kinetic model (*black curves*) to averaged data from wild-type channels (*gray waveforms* and *symbols*). The experimental $Ca^{2+}$-current waveforms (*gray traces*) have been averaged from actual $Ca^{2+}$-current traces in several cells after normalization by peak current amplitude elicited at +10 mV. As displayed, the decay of averaged $Ca^{2+}$ waveforms almost exclusively reflects $Ca^{2+}$ inactivation, because average $Ca^{2+}$ currents have been divided through by smooth exponential fits to similarly averaged $Ba^{2+}$ waveforms (see Methods). Experimental $r_{300}$ and *I-V* relations, shown at right, have been calculated directly from such corrected averages of normalized $Ca^{2+}$ current. Using parameter values as summarized in Table 1, the agreement between kinetic simulation and experimental data is impressive, especially given the simplicity of the model as formulated (Fig. 6 *A*).

To evaluate the feasibility of the proposed transduction role for the consensus EF hand, we examined whether the altered $Ca^{2+}$ inactivation properties induced by mutation in the EF hand could be predicted by adjustment of rate constants that were limited to the transduction step ($B_4 \leftrightarrow I_5$), and to gating transitions closely linked with the target action of the activated EF hand ($C_2 \leftrightarrow O_3$ reaction, by virtue of thin dashed-line interaction in Fig. 6 *A*). V1548Y was chosen for this particular test because the residual $Ca^{2+}$ inactivation was sufficient to quantify with certainty, while the overall reduction in $Ca^{2+}$ inactivation was large. A 5-fold reduction in $k45$ ($B_4 \rightarrow I_5$) largely accounts for the marked effects of the mutation (Fig. 6 *C*), as if the V1548 mutation renders less effective the stabilization of state $I_5$ via the strong interaction between the full-open EF hand and the cytoplasmic gate (Fig. 6 *A*, *thick dashed line*). An additional 2–5-fold slowing of transitions corresponding to the actual opening and closing of the channel ($C_2 \leftrightarrow O_3$) also contributed to the quantitative fits, as if the V1548Y mutation also affected the weak interaction of the consensus EF hand with the cytoplasmic gate (Fig. 6 *A*, *thin dashed line*), thereby influencing the final opening transition of the channel. Table 1 details the precise parameter values for the fits. Overall, the $Ca^{2+}$ inactivation properties of V1548Y are consistent with a transduction role for the consensus EF hand, although such a transduction role is certainly not proven, given the early developmental stage of the model.

## Prediction of a shift between the voltages evoking maximal inactivation versus maximal $Ca^{2+}$ current

An intriguing, but unanticipated, capability of the kinetic model was the ability to predict the shift between the voltage at which $Ca^{2+}$ inactivation is strongest (minimum of $r_{300}$ plot), and the voltage at which the largest peak currents are evoked (Fig. 6 *B*, *s*). This shift was considered to be an important mechanistic clue by Noceti et al. (1998), but what does it mean?

Sherman et al. (1990) deduced that local domain models of $Ca^{2+}$ inactivation would almost invariably predict that inactivation would be strongest at the *same* voltage that elicited the largest peak currents. The theoretical basis for the deduction is surprisingly direct. If activation is fast relative to inactivation (true in our data), then peak current is proportional to $P_{o|A}(V) \times i(V)$, where $i(V)$ is the amplitude of unitary currents at voltage $V$, and $P_{o|A}(V)$ is the conditional probability that the channel will be in the open state ($O_3$) in the steady state at $V$, given that the channel resides in the "active" states (C1, C2, or $O_3$). $P_{o|A}(V) \times i(V)$ will then be proportional to $P_{o|A}(V) \times (V - V_{rev}) = P_{o|A}(V) \times \Delta V$. Under the same assumption of fast activation and slow inactivation, the steady-state extent of $Ca^{2+}$ inactivation increases monotonically with $P_{o|A}(V) \times$ rate constant leading toward inactivated states, which is proportional to $P_{o|A}(V) \times i(V)$ (also proportional to $P_{o|A}(V) \times \Delta V$) in the formulation of Sherman et al. (1990). An analogous argument applies to the rate of $Ca^{2+}$ inactivation. Given that the same voltage-dependent terms ($P_{o|A}(V)$ and $\Delta V$) are present in the expressions for magnitude of peak current and the strength of $Ca^{2+}$ inactivation, peak current and inactivation must be maximal at the same voltage $V$.

Contrary to the expectation of simple local $Ca^{2+}$ domain models, Noceti et al. (1998) observed a clear-cut shift between the voltages where maximal inactivation and peak current were obtained. They could account for the shift,

despite adoption of the local $Ca^{2+}$ domain approximation, by postulating a complex kinetic scheme with 12 states and 3 modes of gating.

However, we also predict such a shift (Fig. 6, *B* and *C*), even though our local $Ca^{2+}$ domain mechanism is simple (Fig. 6 *A*), and should be subject to the clear-cut deduction of Sherman et al. (1990). How is this possible? The answer comes with close re-examination of the term for the steady-state extent of $Ca^{2+}$ inactivation, which will still increase monotonically with $P_{o|A}(V) \times$ rate constant for transition from states 3 to 4. However, because we postulate that CaM binds two $Ca^{2+}$ ions to initiate inactivation, the relevant term now goes as $P_{o|A}(V) \times k34 \times i(V)^2$, where $k34$ is constant with respect to $V$ so that the entire term is thus proportional to $P_{o|A}(V) \times \Delta V^2$. The squaring of the $\Delta V$ term accounts for the dissociation of the peak extent of $Ca^{2+}$ inactivation and the peak current amplitude, because plots of $P_{o|A}(V) \times \Delta V^2$ and $P_{o|A}(V) \times \Delta V$ reach their maxima at different voltages (Fig. 7).

This explanation for the voltage shift pertains to many different detailed reaction schemes for the actual $O_3 \leftrightarrow O_3Ca_2 \leftrightarrow B_4$ reaction, represented in our simulation by a lumped $O_3 \leftrightarrow B_4$ reaction, with a the rightward rate constant proportional to $i(V)^2$ ($\propto [Ca^{2+}]^2_{domain}$). Although our lumped, two-state representation may not map precisely onto the actual functional forms for certain rate-constant regimes of the complete reaction, the important point is that most of the full functional forms will not approximate a single $O_3 \rightarrow B_4$ transition whose rate constant is linearly proportional to $i(V)$, the condition required for coincidence of voltages required for maximal inactivation and maximal $Ca^{2+}$ current. If $Ca^{2+}$ binding to one particular site on CaM becomes rate-limiting in the overall reaction, then the system would manifest such a linear dependence on $i(V)$. However, this scenario seems less likely, as it would not produce the observed voltage shift. In short, it is generally true that the difference in the voltages evoking maximal inactivation and maximal current could arise very simply as a consequence of the multivalent nature of $Ca^{2+}$ binding to the $Ca^{2+}$ sensor.

In this vein, the experimentally observed voltage shift appears to be unchanged in $\alpha_{1C(V1548Y)}$ (Fig. 6 *C*), consistent with presumed mutational effects on transduction rather than on the $Ca^{2+}$ sensor for inactivation. Moreover, mutations at *x*, *y*, *z*, and $-z$ coordinates of the $\alpha_{1C}$ EF-hand motif (Fig. 2) largely preserved the voltage shift, as $Ca^{2+}$ currents all peaked at $\sim +10$ mV. Preservation of the shift accords with a weak (or absent) role for low-affinity $Ca^{2+}$ binding to the EF hand in modulating the overall $Ca^{2+}$ responsiveness of inactivation, as assumed for the simulations in Fig. 6. Finally, close inspection of the predicted and actual shifts in Fig. 6, *B* and *C* raises a provocative suggestion. The model consistently underestimates the extent of shift in experimental data, and further simulation indicates that the predicted shift could become progressively larger as the

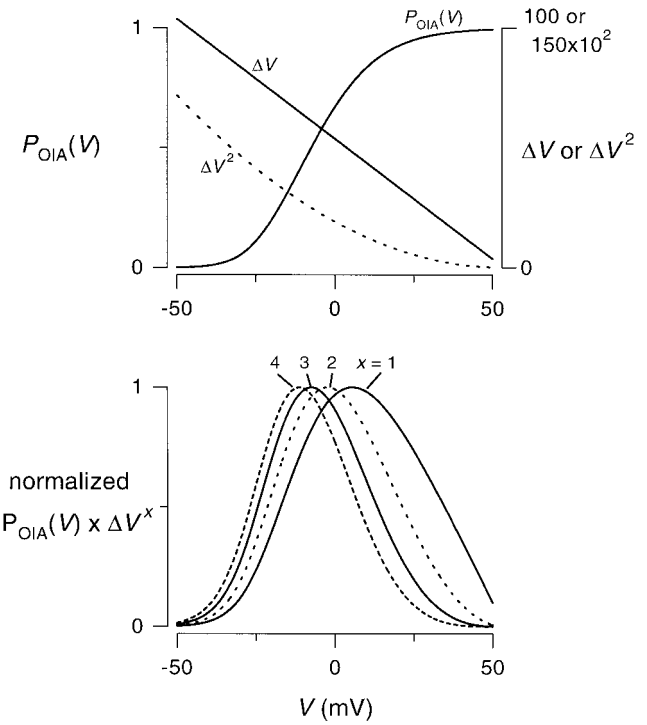


FIGURE 7 Potential explanation for the shift in voltage required to evoke maximal $Ca^{2+}$ and maximal $Ca^{2+}$-dependent inactivation. *Top:* plots of $P_{O|A}(V)$, $\Delta V$, and $\Delta V^2$, all as a function of step potential. $P_{O|A}(V)$, the steady-state open probability of the "active states" within the wild-type channel, was calculated for the wild-type subsystem $C_1 \leftrightarrow C_2 \leftrightarrow O_3$ as given in Table 1. $\Delta V$ and $\Delta V^2$ were calculated from $(V - V_{reversal})$ and $(V - V_{reversal})^2$, respectively, where $V_{reversal}$ was 53.7 mV as determined for the wild-type channel in Table 1. The magnitude of peak $Ca^{2+}$ current as a function of step potential is proportional to the product of $P_{O|A}(V)$ and $\Delta V$ curves. The 100-mV scale on the right pertains to the $\Delta V$ curve, and the $150 \times 10^2$-mV$^2$ scale to the $\Delta V^2$ curve. For channels in which the binding of one $Ca^{2+}$ ion alone initiates $Ca^{2+}$ inactivation, the strength of $Ca^{2+}$ inactivation is proportional to the same product. If the binding of two $Ca^{2+}$ ions initiates $Ca^{2+}$ inactivation, and this is reflected by an $O_3 \rightarrow B_4$ rate constant proportional to $[Ca^{2+}]^2_{domain}$, then the strength of $Ca^{2+}$ inactivation is proportional to the product of $P_{O|A}(V)$ and $\Delta V^2$ curves. *Bottom:* normalized products of $P_{O|A}(V)$ and $\Delta V^x$, plotted as a function of voltage, where $x$ is an integer power term. The peak of these curves resides at increasingly hyperpolarized potentials as the power term $x$ increases. The plot of peak $Ca^{2+}$ current versus voltage will always be proportional to the curve corresponding to $x = 1$. For the case where the binding of one $Ca^{2+}$ ion produces $Ca^{2+}$ inactivation, the strength of $Ca^{2+}$ inactivation will also be monotonically related to the curve corresponding to $x = 1$. Hence, the same voltage will evoke maximal $Ca^{2+}$ current and maximal $Ca^{2+}$ inactivation. If, however, the binding of two $Ca^{2+}$ ions initiates $Ca^{2+}$ inactivation, and this is reflected by an $O_3 \rightarrow B_4$ rate constant proportional to $[Ca^{2+}]^2_{domain}$, then the strength of inactivation will be related monotonically to the curve for $x = 2$, which peaks at a more negative voltage than does the curve for $x = 1$. Hence, the voltage at which maximal $Ca^{2+}$ inactivation occurs will be more negative than the voltage at which maximal peak $Ca^{2+}$ current is observed. If the binding of 3 or 4 $Ca^{2+}$ ions initiates $Ca^{2+}$ inactivation, and this can be approximated by an $O_3 \rightarrow B_4$ rate constant proportional to $[Ca^{2+}]^3_{domain}$ or $[Ca^{2+}]^4_{domain}$, then the strength of $Ca^{2+}$ inactivation will be monotonically related to the curves for $x = 3$ or $x = 4$, respectively. This results in further left-shifting of the voltage at which maximal inactivation is observed.

valency of $Ca^{2+}$ binding is increased to 3 or 4 (Fig. 7). In fact, the experimentally observed shift is better fit by models assuming a valency of four $Ca^{2+}$ ions. Yet, our previous results argue that $Ca^{2+}$ binding to only the C-terminal lobe of CaM (with two $Ca^{2+}$ sites) is necessary for $Ca^{2+}$ inactivation (Peterson et al., 1999). Could two CaM molecules serve as $Ca^{2+}$ sensor for L-type channel inactivation?

Carla D. DeMaria provided insightful comments and discussion. We thank E. Perez-Reyes for the $\alpha_{1C}$ and $\beta_{2a}$ clones, and T. P. Snutch for the $\alpha_2\delta$ construct.

This work was supported by grants from the National Institutes of Health (to D.T.Y.).

## REFERENCES

Adams, B., and T. Tanabe. 1997. Structural regions of the cardiac Ca channel alpha subunit involved in Ca-dependent inactivation. *J. Gen. Physiol.* 110:379–389.

Ames, J. B., R. Ishima, T. Tanaka, J. I. Gordon, L. Stryer, and M. Ikura. 1997. Molecular mechanics of calcium-myristoyl switches. *Nature.* 389: 198–202.

Babitch, J. 1990. Channel hands. *Nature.* 346:321–322.

Bernatchez, G., D. Talwar, and L. Parent. 1998. Mutations in the EF-hand motif impair the inactivation of barium currents of the cardiac alpha1C channel. *Biophys. J.* 75:1727–1739.

Brehm, P., and R. Eckert. 1978. Calcium entry leads to inactivation of calcium channel in *Paramecium. Science.* 202:1203–1206.

Chazin, W. J. 1995. Releasing the calcium trigger. *Nat. Struct Biol.* 2:707–710.

Deisseroth, K., H. Bito, and R. W. Tsien. 1996. Signaling from synapse to nucleus: postsynaptic CREB phosphorylation during multiple forms of hippocampal synaptic plasticity. *Neuron.* 16:89–101.

de Leon, M., Y. Wang, L. Jones, E. Perez-Reyes, X. Wei, T. W. Soong, T. P. Snutch, and D. T. Yue. 1995. Essential $Ca^{2+}$-binding motif for $Ca^{2+}$-sensitive inactivation of L-type $Ca^{2+}$ channels. *Science.* 270: 1502–1506.

De Waard, M., C. A. Gurnett, and K. P. Campbell. 1996. Structural and functional diversity of voltage-activated calcium channels. *In* Ion Channels. T. Narahashi, editor. Plenum Press, New York. 41–87.

Falke, J. J., S. K. Drake, A. L. Hazard, and O. B. Peersen. 1994. Molecular tuning of ion binding to calcium signaling proteins. *Q. Rev. Biophys.* 27:219–290.

Ferreira, G., J. Yi, E. Rios, and R. Shirokov. 1997. Ion-dependent inactivation of barium current through L-type calcium channels. *J. Gen. Physiol.* 109:449–461.

Flaherty, K. M., S. Zozulya, L. Stryer, and D. B. McKay. 1993. Three-dimensional structure of recoverin, a calcium sensor in vision. *Cell.* 75:709–716.

Herzberg, O., J. Moult, and M. N. James. 1986. A model for the $Ca^{2+}$-induced conformational transition of troponin C. A trigger for muscle contraction. *J. Biol. Chem.* 261:2638–2644.

Ho, S., H. Hunt, R. Horton, J. Pullen, and L. Pease. 1989. Site-directed mutagenesis by overlap extension using the polymerase chain reaction. *Gene.* 77:51–59.

Imredy, J. P., and D. T. Yue. 1992. Submicroscopic $Ca^{2+}$ diffusion mediates inhibitory coupling between individual $Ca^{2+}$ channels. *Neuron.* 9:197–207.

Imredy, J. P., and D. T. Yue. 1994. Mechanism of $Ca^{2+}$-sensitive inactivation of L-type $Ca^{2+}$ channels. *Neuron.* 12:1301–1318.

Jones, L. P., S. K. Wei, and D. T. Yue. 1998. Mechanism of auxiliary subunit modulation of neuronal $\alpha_{1E}$ calcium channels. *J. Gen. Physiol.* 112:125–143.

Kass, R. S., and M. Sanguinetti. 1984. Inactivation of calcium channel current in the calf cardiac Purkinje fiber. Evidence for voltage- and calcium-mediated mechanisms. *J. Gen. Physiol.* 84:705–726.

Klockner, U., G. Mikala, M. Varadi, G. Varadi, and A. Schwartz. 1995. Involvement of the carboxyl-terminal region of the alpha 1 subunit in voltage-dependent inactivation of cardiac calcium channels. *J. Biol. Chem.* 270:17306–17310.

Larsson, H. P., O. S. Baker, D. S. Dhillon, and E. Y. Isacoff. 1996. Transmembrane movement of the *Shaker* $K^+$ channel S4. *Neuron.* 16:387–397.

Lee, K., E. Marban, and R. W. Tsien. 1985. Inactivation of calcium channels in mammalian heart cells: joint dependence on membrane potential and intracellular calcium. *J. Physiol.* 364:395–411.

Lee, A., S. T. Wong, D. Gallagher, B. Li, D. R. Storm, T. Scheuer, and W. A. Catterall. 1999. $Ca^{2+}$/calmodulin binds to and modulates P/Q-type calcium channels. *Nature.* 399:155–159.

Linse, S., and S. Forsen. 1995. Determinants that govern high-affinity calcium binding. *Adv. Second Messenger Phosphoprotein Res.* 30: 89–151.

Linz, K. W., and R. Meyer. 1998. Control of L-type calcium current during the action potential of guinea-pig ventricular myocytes. *J. Physiol.* 513:425–442.

Liu, Y., M. Holmgren, M. E. Jurman, and G. Yellen. 1997. Gated access to the pore of a voltage-dependent $K^+$ channel. *Neuron.* 19:175–184.

Noceti, F., R. Olcese, N. Qin, J. Zhou, and E. Stefani. 1998. Effect of bay K 8644 (−) and the beta2a subunit on $Ca^{2+}$-dependent inactivation in alpha1C $Ca^{2+}$ channels. *J. Gen. Physiol.* 111:463–475.

O'Rourke, B., D. A. Kass, G. F. Tomaselli, S. Kaab, R. Tunin, and E. Marban. 1999. Mechanisms of altered excitation-contraction coupling in canine tachycardia-induced heart failure: I. Experimental study. *Circ. Res.* 84:562–570.

Patil, P. G., D. L. Brody, and D. T. Yue. 1998. Preferential closed-state inactivation of neuronal calcium channels. *Neuron.* 20:1027–1038.

Perez-Reyes, E., A. Castellano, H. S. Kim, P. Bertrand, E. Baggstrom, A. E. Lacerda, X. Y. Wei, and L. Birnbaumer. 1992. Cloning and expression of a cardiac/brain beta subunit of the L- type calcium channel. *J. Biol. Chem.* 267:1792–1797.

Perez-Reyes, E., and T. Schneider. 1994. Calcium channels: structure, function, and classification. *Drug Dev. Res.* 33:295–318.

Perozo, E., D. M. Cotes, and L. G. Cuello. 1999. Structural rearrangements underlying $K^+$-channel activation gating. *Science.* 285:73–78.

Peterson, B. Z., C. D. DeMaria, J. P. Adelman, and D. T. Yue. 1999. Calmodulin is the $Ca^{2+}$ sensor for $Ca^{2+}$-dependent inactivation of L-type calcium channels. *Neuron.* 22:549–558.

Qin, N., R. Olcese, M. Bransby, T. Lin, and L. Birnbaumer. 1999. $Ca^{2+}$-induced inhibition of the cardiac $Ca^{2+}$ channel depends on calmodulin. *Proc. Natl. Acad. Sci. USA.* 96:2435–2438.

Rhoads, A. R., and F. Friedberg. 1997. Sequence motifs for calmodulin recognition. *FASEB J.* 11:331–340.

Sherman, A., J. Keizer, and J. Rinzel. 1990. Domain model for $Ca^{2+}$-inactivation of $Ca^{2+}$ channels at low channel density. *Biophys. J.* 58: 985–995.

Shirokov, R. E., R. Levis, N. Shirokova, and E. Rios. 1993. $Ca^{2+}$-dependent inactivation of cardiac L-type Ca2+ channels does not affect their voltage sensor. *J. Gen. Physiol.* 102:1005–1030.

Simon, S., and R. Llinas. 1985. Compartmentalization of the submembrane calcium activity during calcium influx and its significance in transmitter release. *Biophys J.* 48:485–498.

Singer-Lahat, D., I. Lotan, K. Itagaki, A. Schwartz, and N. Dascal. 1992. Evidence for the existence of RNA of $Ca^{2+}$-channel alpha 2/delta subunit in *Xenopus* oocytes. *Biochim. Biophys. Acta.* 1137:39–44.

Soldatov, N. M., M. Oz, K. A. O'Brien, D. R. Abernethy, and M. Morad. 1998. Molecular determinants of L-type $Ca^{2+}$ channel inactivation. Segment exchange analysis of the carboxyl-terminal cytoplasmic motif encoded by exons 40–42 of the human alpha1C subunit gene. *J. Biol. Chem.* 273:957–963.

Soldatov, N. M., R. D. Zuhlke, A. Bouron, and H. Reuter. 1997. Molecular structures involved in L-type calcium channel inactivation. Role of the

carboxyl-terminal region encoded by exons 40–42 in alpha1C subunit in the kinetics and $Ca^{2+}$ dependence of inactivation. *J. Biol. Chem.* 272: 3560–3566.

Soong, T. W., A. Stea, C. D. Hodson, S. J. Dubel, S. R. Vincent, and T. P. Snutch. 1993. Structure and functional expression of a member of the low voltage-activated calcium channel family. *Science.* 260:1133–1136.

Standen, N., and P. Stanfield. 1982. A binding-site model for calcium channel inactivation that depends on calcium entry. *Proc. R. Soc. (Lond).* 217:101–110.

Tanaka, T., J. B. Ames, T. S. Harvey, L. Stryer, and M. Ikura. 1995. Sequestration of the membrane-targeting myristoyl group of recoverin in the calcium-free state. *Nature.* 376:444–447.

Tomlinson, W. J., A. Stea, E. Bourinet, P. Charnet, J. Nargeot, and T. P. Snutch. 1993. Functional properties of a neuronal class C L-type calcium channel. *Neuropharmacology*. 32:1117–1126.

Villain, M., P. Jackson, W. J. Dong, D. Muccio, and J. E. Blalock. 1999. Characterization of an atypical $Ca^{2+}$ binding motif from L-type $Ca^{2+}$ channels. *Biophys. J.* 76:101*a*. (Abstr.).

Walker, D., and M. De Waard. 1998. Subunit interaction sites in voltage-dependent $Ca^{2+}$ channels: role in channel function. *Trends. Neurosci.* 21:148–154.

Wei, X. Y., E. Perez-Reyes, A. E. Lacerda, G. Schuster, A. M. Brown, and L. Birnbaumer. 1991. Heterologous regulation of the cardiac $Ca^{2+}$ channel alpha 1 subunit by skeletal muscle beta and gamma subunits. Implications for the structure of cardiac L-type $Ca^{2+}$ channels. *J. Biol. Chem.* 266:21943–21947.

Winslow, R., J. Rice, S. Jafri, E. Marban, and B. O'Rourke. 1999. Mechanisms of altered excitation-contraction coupling in canine tachycardia-induced heart failure: II. Model study. *Circ. Res.* 84:571–586.

Yang, N., and R. Horn. 1996. Molecular basis of charge movement in voltage-gated sodium channels. *Neuron.* 16:113–122.

Zhang, J. F., P. T. Ellinor, R. W. Aldrich, and R. W. Tsien. 1994. Molecular determinants of voltage-dependent inactivation in calcium channels. *Nature.* 372:97–100.

Zhou, J., R. Olcese, N. Qin, F. Noceti, L. Birnbaumer, and E. Stefani. 1997. Feedback inhibition of $Ca^{2+}$ channels by $Ca^{2+}$ depends on a short sequence of the C terminus that does not include the $Ca^{2+}$ - binding function of a motif with similarity to $Ca^{2+}$-binding domains. *Proc. Natl. Acad. Sci. USA.* 94:2301–2305.

Zozulya, S., and L. Stryer. 1992. Calcium-myristoyl protein switch. *Proc. Natl. Acad. Sci. USA.* 89:11569–11573.

Zuhlke, R. D., G. S. Pitt, K. Deisseroth, R. W. Tsien, and H. Reuter. 1999. Calmodulin supports both inactivation and facilitation of L-type calcium channels. *Nature.* 399:159–162.

Zuhlke, R. D., and H. Reuter. 1998. $Ca^{2+}$-sensitive inactivation of L-type $Ca^{2+}$ channels depends on multiple cytoplasmic amino acid sequences of the $\alpha_{1c}$ subunit. *Proc. Natl. Acad. Sci. USA.* 95:3287–3294.